Missouri University of Science and Technology

Scholars' Mine

Civil, Architectural and Environmental Engineering Faculty Research & Creative Works

Civil, Architectural and Environmental Engineering

01 Apr 2023

# Analysis of Eccentrically Loaded FRP Partially Wrapped Reinforced Concrete Columns Subjected to Combined Environmental Erosion

Zhiqiang Gu

Congjie Wei

Chenglin Wu
*Missouri University of Science and Technology*, wuch@mst.edu

Danying Gao

*et. al. For a complete list of authors, see https://scholarsmine.mst.edu/civarc_enveng_facwork/2383*

Follow this and additional works at: https://scholarsmine.mst.edu/civarc_enveng_facwork

 Part of the Architectural Engineering Commons, and the Civil and Environmental Engineering Commons

## Recommended Citation

Z. Gu et al., "Analysis of Eccentrically Loaded FRP Partially Wrapped Reinforced Concrete Columns Subjected to Combined Environmental Erosion," *Engineering Structures*, vol. 280, article no. 115720, Elsevier, Apr 2023.
The definitive version is available at https://doi.org/10.1016/j.engstruct.2023.115720

This Article - Journal is brought to you for free and open access by Scholars' Mine. It has been accepted for inclusion in Civil, Architectural and Environmental Engineering Faculty Research & Creative Works by an authorized administrator of Scholars' Mine. This work is protected by U. S. Copyright Law. Unauthorized use including reproduction for redistribution requires the permission of the copyright holder. For more information, please contact scholarsmine@mst.edu.

Engineering Structures 280 (2023) 115720

Contents lists available at ScienceDirect

Engineering Structures

journal homepage: www.elsevier.com/locate/engstruct

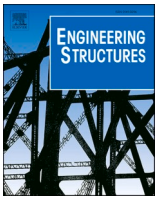

# Analysis of eccentrically loaded FRP partially wrapped reinforced concrete columns subjected to combined environmental erosion

Zhiqiang Gu [a], Congjie Wei [b], Chenglin Wu [b], Danying Gao [a,*], Peibo You [c], Dong Wei [a]

[a] Yellow River Laboratory, Zhengzhou University, Zhengzhou 450001, China
[b] Department of Civil, Architectural, and Environmental Engineering, Missouri University of Science and Technology, Rolla, MO, USA
[c] School of Civil and Transport Engineering, Henan University of Urban Construction, Pingdingshan 467000, China

ARTICLE INFO

*Keywords:*
FRP partially wrapped
Corroded RC column
Eccentric loading
Analytical model
Freeze-thaw erosion

ABSTRACT

The behavior of eccentrically loaded fiber reinforced polymer (FRP) partially wrapped reinforced concrete (RC) columns under combined environmental erosion was investigated in this paper. Circular RC columns were firstly subjected to chloride erosion where the target corrosion degree (0, 10 %, and 20 %) is obtained with externally applied current. This was then followed by partially strengthening with 2-ply of glass fiber reinforced polymer (GFRP) strips as well as 50 freeze–thaw cycles. Series of eccentric compression tests were conducted with ranging eccentricities of 0, 5 mm, 10 mm, and 15 mm. For comparison, the carbon fiber reinforced polymer (CFRP) partially strengthened columns with the corrosion degree of 10 % and subjected to 50 freeze–thaw cycles were also eccentrically loaded with an eccentricity of 10 mm. Results showed that with increasing corrosion degree, the bearing capacity of GFRP strengthened column showed a 2-stage behavior (firstly increased and then decreased), which may be caused by the confinement reduction of FRP on columns due to severe environmental erosion. Under small eccentric loading, The CFRP strengthened RC columns showed better compressive behavior than that of GFRP strengthened RC columns. Based on the stress–strain relationship of constituent materials, a simplified analytical model considered the effects of chloride and freeze–thaw erosion was put forward to predict the bearing capacity of FRP partially wrapped RC column under eccentric loading.

## 1. Introduction

Reinforced concrete (RC) column exposure to humidity environmental could be easily corroded and develop corrosion damages that lead to the reinforcement deterioration, including reduction of tensile capacity and failure elongation. Furthermore, radial stress caused by the expansion of corrosion products could result in tensile cracking of concrete and significantly decrease the mechanical properties and durability of RC columns [1–3]. Repairing and strengthening of corrosion damaged RC column has always been a hotspot in related engineering fields.

Externally bonded fiber reinforced polymer (FRP) was considered as one of the most effective way to strengthening the corrosion damaged RC columns. A considerable amount of studies have been carried out about the compressive behavior of FRP strengthening damaged RC columns [4–7]. It is found that FRP strengthening could significantly decrease the corrosion rate of steel bars in column [8], and improve the durability, ductility, stiffness, and load capacity of damaged columns [9–11]. The effectiveness of FRP strengthening damaged columns subjected to axial compression loading has been validated. Under realistic conditions, however, concrete columns are often applied combined flexural and axial loading, which could accelerate corrosion induced crack initiation and propagation once corroded. Serviceability could then be significantly compromised during this process. Maaddawy [12] studied the effectiveness of carbon fiber reinforced polymer (CFRP) strengthening in the corrosion process of eccentrically loaded RC columns. In this research, the columns with steel mass loss of 4.25 % were strengthened by CFRP and subjected to eccentric loading with different eccentricity. Results showed that the bearing capacity of strengthened columns decreased proportionally with the increasing eccentricity ratio while the bearing capacity corresponding to the corrosion damaged column fully wrapped with CFRP was 40 % higher than that of the uncorroded column. Moreover, the confinement effect of CFRP decreased with the increasing eccentricity ratio. Jayaprakash et al. [13] reported that the load capacities of FRP confined corrosion damaged RC circular column were increased from 8 % to 36 % for mild corrosion level and 21

* Corresponding author.
*E-mail address:* gaodanyingzzu@126.com (D. Gao).

https://doi.org/10.1016/j.engstruct.2023.115720
Received 16 November 2022; Received in revised form 25 January 2023; Accepted 26 January 2023
Available online 4 February 2023
0141-0296/© 2023 Elsevier Ltd. All rights reserved.

% to 34 % for severe corrosion level when compared with the unconfined damaged columns under eccentric loading. Tin [14] investigated the influences of steel corrosion on the FRP strengthened column subjected to eccentric loading. Twenty-four rectangular RC columns with different corrosion degrees were strengthened with different number of FRP layers. Test results indicated that the ratio of bearing capacity of FRP strengthened corrosion damaged RC columns to that of corresponding controlled columns increases proportionally with the increasing corrosion degree, and it slightly increases with the increasing eccentricity and FRP layer as well. Comparing with the corresponding controlled columns, the ultimate vertical displacement of strengthened columns is negatively correlated with the increasement of corrosion degree, and noticeably with the increasement of FRP layer and eccentricity. Chotickai et al. [15] conducted the test of CFRP strengthened corrosion damaged RC columns under eccentric loading. Results showed that CFRP could significantly improve the structural behavior including stiffness, ductility, and bearing capacity of columns, while the improvement effect decreases with the increasing corrosion degree. It is also reported that the load capacity improvement and the confinement effects are both positively correlated to the volumetric CFRP ratio of CFRP jacket.

These abovementioned works confirmed the effectiveness of FRP strengthening on improving the structural performance of RC columns when corrosion damage is introduced. However, the RC columns in reality project are often subjected to complex environment including chloride erosion as well as freeze–thaw erosion when served in humid and cold regions [16]. When severely corroded, extra channels for water penetration would develop in columns by the corrosion cracks, and in turn enhances the crack propagation due to the expansion stress of freezing water under freeze–thaw cycling. This cyclic process seriously decreases the service life of columns and makes the RC columns exposed to combine environmental erosion one of the most essential problems in engineering. However, the eccentric compressive mechanical behavior of FRP strengthened RC columns served in the combined chloride and freeze–thaw erosion environments, which could have complex stress states, are mostly studied using numerical approaches that are difficult to apply to engineering design [17–20]. Comparingly, experimental and analytical studies and related research are rarely reported to date [10,16,21]. Maaddawy [22] proposed a nonlinear second-order analysis method to predict the strength of eccentrically loaded RC columns wrapped with CFRP, which considered the additional eccentricity caused by lateral deformation and validated by the experimental results. Al-Nimry [23] adopted the *ACI* 440.2R design guidelines [24] to analyze the axial-flexural interactions of FRP confined RC column and found that the calculated results were slightly conservative. Based on test data, Chotickai [15] considered the influence of steel corrosion and proposed a mechanical property model to calculate the capacity of CFRP strengthened corroded rectangular RC columns under eccentric loading. However, to the best of the authors' knowledge, a capacity prediction method for FRP strengthened RC columns that take consideration of combined influences of chloride and freeze–thaw erosion under eccentric loading has not been reported yet. The analytical model about the bearing capacity prediction of eccentrically loaded FRP strengthened RC columns under combined environmental erosion is urgently needed for engineering design.

Upon this background, in this study, 48 small-scale circular FRP partially wrapped RC columns were tested under small eccentric loading conditions. The combined chloride and freeze–thaw erosion were applied to the columns. The main parameters were set as reinforcement corrosion degree, FRP types, and eccentricities to study the influences of combined environmental erosion and eccentricity on the structural behavior of column. Based on the stress–strain relationships of FRP confined concrete and steel bar subjected to combined environmental erosion, a section analysis method was proposed and used to calculate the load capacity of FRP confined RC columns exposed to chloride and freeze–thaw erosion. Results showed that the simplified analytical model could predict the bearing capacity of columns within experiments.

## 2. Test program

### 2.1. Specimen design and material properties

A total of 16 groups of specimens were prepared in this experiment. Each group contained three identical columns. The designed corrosion degree of steel bars in the column was set as 0, 10 %, and 20 %, respectively. 50 freeze–thaw cycles were conducted for all columns after chloride erosion while glass fiber reinforced polymer (GFRP) and CFRP were both considered as reinforcements. 3 sets of eccentricities were considered as 0, 5 mm, 10 mm, and 15 mm, respectively. Detailed parameters setups are listed in Table 1, where specimen groups are referred with a name starting with the capital letter "G" or "C" to indicate the type of adopted FRP ("G" for GFRP and "C" for CFRP) and followed by a number to indicate the number of FRP layers. The abbreviations "CR" followed by a number after the dash sign is used to indicate the corrosion degree. The last number after the second dash sign indicates the eccentricity. As an example, *C*2-CR10-10 refers to CFRP strengthened column with the steel bar corrosion degree of 10 %, freeze–thaw cycles of 50, and eccentricity of 10 mm.

The compressive strength of concrete used for all columns was 31.5 MPa. The circular columns were designed to have a 400 mm height, 100 mm section diameter, as well as a concrete cover thickness of 25 mm. Four 8 mm plain bars were used as longitudinal reinforcement, and 6 mm plain bars with a spacing of 70 mm were used as stirrups. The yielding strength of the reinforcements was 235 MPa and elastic modulus 210 GPa. All columns were partially wrapped with two plies of 30 mm wide FRP strip and the strip spacing was set as 70 mm, as shown in Fig. 1. The overlapping zone of the FRP strip was set as 150 mm to avoid bond slip failure.

### 2.2. Specimen preparation

The RC columns were firstly submerged into a 5 % saline solution while an accelerated corrosion method according to Faraday's law was used in this study: the electrical potential was set as 15 V and the current density of reinforcement in columns was controlled at 0.5 mA/cm$^2$ [5]. The accelerated corrosion setup is presented in Fig. 2.

**Table 1**
The detailed parameters of specimen.

| Specimen ID | Number of FRP layers | Steel bar corrosion degree (%) | Freeze-thaw cycles | Eccentricity (mm) |
|---|---|---|---|---|
| G2-CR0-0 | 2 | 0 | 50 | 0 |
| G2-CR0-5 | 2 | 0 | 50 | 5 |
| G2-CR0-10 | 2 | 0 | 50 | 10 |
| G2-CR0-15 | 2 | 0 | 50 | 15 |
| G2-CR10-0 | 2 | 10 | 50 | 0 |
| G2-CR10-5 | 2 | 10 | 50 | 5 |
| G2-CR10-10 | 2 | 10 | 50 | 10 |
| G2-CR10-15 | 2 | 10 | 50 | 15 |
| G2-CR20-0 | 2 | 20 | 50 | 0 |
| G2-CR20-5 | 2 | 20 | 50 | 5 |
| G2-CR20-10 | 2 | 20 | 50 | 10 |
| G2-CR20-15 | 2 | 20 | 50 | 15 |
| C2-CR10-0 | 2 | 10 | 50 | 0 |
| C2-CR10-5 | 2 | 10 | 50 | 5 |
| C2-CR10-10 | 2 | 10 | 50 | 10 |
| C2-CR10-15 | 2 | 10 | 50 | 15 |

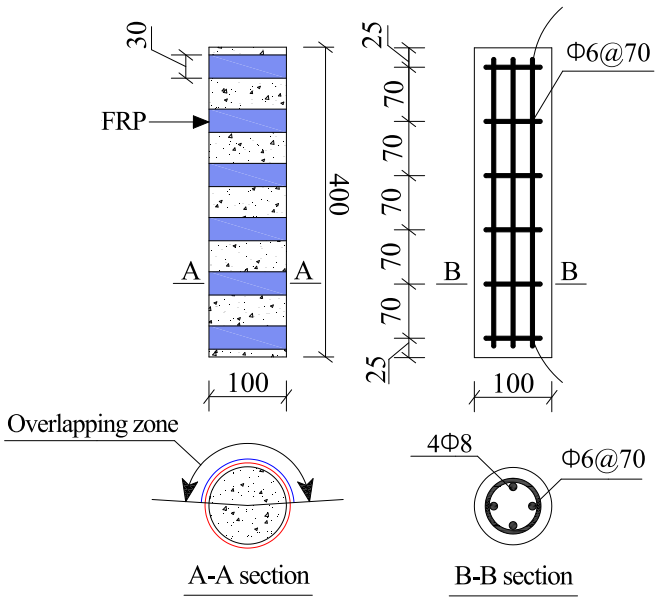


**Fig. 1.** Reinforcement diagram of FRP partially wrapped column.

**Fig. 2.** Accelerated corrosion setup.

After the target theoretical corrosion degree was reached, the columns were wrapped with two plies of FRP strip by using wet-layup method where the fiber orientation of FRP strip was designed to coincide with the hoop direction. The saturating resin used for the FRP wraps was epoxy resin with polyamine hardener, it has a tensile shear strength of 24.29 MPa, tensile strength of 40.12 MPa, compressive strength of 73.62 MPa, bending strength of 72.95 MPa, elastic modulus of 2605.7 MPa, and elongation of 2.45 %. For corrosion damaged RC columns, the chloride ions had already penetrated into the column and fully wrapping FRP could not prevent the further corrosion of reinforcement [12]. Therefore, FRP partial wrapping technique was used in this experiment. Fig. 3 presents the CFRP partially wrapped RC columns before freeze–thaw erosion.

The rapid freezing-thawing experiment approach [25] was used in this work and the freeze–thaw cycles were set as 50 for all columns. In this experiment, the concrete prisms with the dimension of 150 mm × 150 mm × 300 mm were cast simultaneously with the RC columns to test the axial compressive strength and elastic modulus of concrete. To investigate the effects of freeze–thaw erosion on the mechanical properties of materials and provide test data for column bearing capacity calculation, the FRP strips and concrete prisms used in this work were also subjected to 50 freeze–thaw cycles, respectively. The detailed specimen preparation process could be found in the published work of authors [21].

**Fig. 3.** CFRP partially wrapped columns before freeze–thaw erosion.

### 2.3. Experimental setup and instrumentation

The tensile test of FRP strips was conducted through a 50 kN testing machine [26]. As for the concrete prisms, compression tests of specimens were conducted through a 3000 kN testing machine [27] while that of columns was through a 2000 kN testing machine. Multistage loading procedures were adopted, and each step was sustained 3 min before data collection. Fig. 4 presents the column test setup and instrumentation. The loading plates with knife edge were used to achieve the desired eccentricity. The axial displacement of column was measured by two linear voltage differential transformers (LVDTs). In this paper, the compressive strains of column are defined to be positive.

## 3. Results and discussion

### 3.1. Actual corrosion degrees of the steel bar, and mechanical properties of the constituent materials

After the failure of columns under compression, the corroded steel bars were extracted from column and cleaned with hydrochloric acid solution to test the actual corrosion degrees. Results showed that the actual steel mass losses of 10 % corrosion degree steel bar were 15.44 % and 20 % corrosion degree steel bar 19.24 %. The detailed explanation of this phenomenon could be found in Appendix A. The actual corrosion degrees of steel bar were adopted in following discussion and calculation.

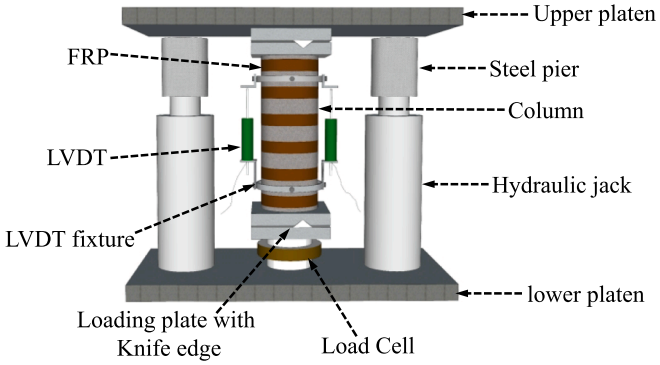


**Fig. 4.** Test setup and instrumentations of the column.

The mechanical properties of FRP strips, including tensile strength ($\sigma_t$), elastic modulus ($E_t$), and elongation ($\varepsilon_t$) are listed in Table 2, along with all the coefficient of variations (COV). It could be seen that both the GFRP and CFRP tensile strengths decrease after freeze–thaw cycling, while the variation of the elastic modulus of FRP strips is not obvious. And the elongation of GFRP and CFRP strips slightly decreased after freeze–thaw cycles. The tensile strengths of GFRP and CFRP strips after 50 freeze–thaw cycles were decreased by 3.29 % and 1.7 % compared with that of the GFRP and CFRP strips without freeze–thaw erosion, respectively. It was found that the freeze–thaw erosion on the GFRP trips has a more significant influence due to the reason that GFRP has a higher capability of absorbing water than that of CFRP [28]. Under freeze–thaw condition, freezing water introduces expansion stress to degrade the interfacial bonding between the glass fiber and base resin as well as weaken the effect of base resin to the shear stress transfer capacity, strength, and deformation of GFRP strip. The freeze–thaw erosion also has serious effects on the concrete properties, showing as a decreased axial compressive strength from 31.5 MPa to 26.9 MPa after 50 freeze–thaw cycles.

### 3.2. Failure mode

Fig. 5 presents the typical failure modes of columns. All columns exhibited ductile failure regardless of the eccentricity. For columns under axial compression loading, compressive stress is uniformly distributed throughout the section. In early loading stage, the compressive load was mainly borne by longitudinal reinforcement and concrete while the confining effect of the FRP was neglectable. When the column reached the ultimate load capacity, concrete crush was observed, and the load capacity of column started to decrease gradually. Due to the constraint provided by FRP strip, the failure mode of axial compression loaded columns changed from brittle to ductile. For eccentrically loaded columns, the section of column was all in compression firstly. With the load increasing, the depth of compression zone of column section decreased while the constraint stress provided by FRP strip increased. When ultimate load of column was reached, concrete crush first appeared in compression zone and lead to the failure of FRP strips. The column exhibited good ductility under eccentric loading. Besides, it was found that the failure modes of GFRP strips were splitting or tearing broken while the CFRP adopted tensile failure modes with neat or serrated sections. The saturating resin used for GFRP and CFRP was same, while the elongation capability of glass fiber was higher than that of carbon fiber, which results in a reduced interfacial bonding between glass fibers and saturating resin than that of carbon fibers and saturating resin. Therefore, the GFRP strip presented the tearing and peeling failure mode between fibers and saturating resin.

### 3.3. Bearing capacity

Fig. 6 presents the bearing capacity of columns. As shown, the bearing capacity decreased with the increasing eccentricity regardless of the corrosion degree and FRP types. For GFRP strengthened un-corroded series columns (G2-CR0-n series), the bearing capacity of columns with different eccentricities of 5 mm, 10 mm, and 15 mm were 11.8 %, 22 %, and 29 % less than that of the axial compression loaded column, respectively. For CFRP strengthened columns (*C*2-CR10-n series), the bearing capacity of columns with the eccentricities of 5 mm, 10 mm, and 15 mm were 12.2 %, 22.5 %, and 30.9 % less than that of the axial compression loaded column, respectively. It was found that the decreasing effect on the load capacity of FRP strengthened columns decreases with increasing eccentricity. The main reason was that for small eccentric loaded columns, the expansive deformation of concrete and the constraint stress provided by FRP strips were relatively low under the ultimate limit state. With the increasing eccentricity, the constraining effect provided by the FRP strips increases and partially neutralizes decreasing effect caused by the corrosion.

Besides, the bearing capacity of GFRP strengthened damaged columns under the same eccentric loading presented a 2-stage trend (firstly increase and then decrease) with the increasing reinforcement corrosion degree, as shown in Fig. 6. Compared to the GFRP strengthened un-corroded columns under axial compression loading, the bearing capacities of GFRP strengthened corrosion damaged RC column with different corrosion degrees of 15.44 % and 19.24 % were decreased −5.5 % and 8.8 % under axial compression loading, respectively. Compared to GFRP strengthened un-corroded RC columns under the eccentricity of 10 mm, the bearing capacities of GFRP strengthened corrosion RC column with different corrosion degrees of 15.44 % and 19.24 % were decreased −6.5 % and 6.2 % under the eccentricity of 10 mm, respectively. The main reasons could be summarized as follows: 1) after reaching the 28-day curing age, the columns were immediately submerged into the 5 % saline solution, which could further promote the hydration of concrete and slightly improve the mechanical properties of concrete; 2) for mild corroded reinforcement, the corrosion products on the reinforcement surface were conducive to the compaction of the steel–concrete interface, thereby improve the bond strength between reinforcement and concrete [29,30]. Moreover, for FRP confined corroded RC columns, the restraint provided by FRP strips could increase the internal pressure of concrete and restrain the micro-crack propagation caused by expansion of corrosion products, thereby the strengthening mechanism of bond stress between the corroded reinforcement and concrete became more significant [31]; 3) the relatively low concrete strength results in more internal pores. During the chloride corrosion, the corrosion products could partially fill the pores of concrete and the compactness of concrete was improved [32], which could prevent the freezing water goes into the core region of column and reduce the freeze–thaw damage of columns to some extent. Therefore, the bearing capacity of columns presented the increasing trend for moderate corroded RC columns. However, for severely corroded columns, the expansion stress caused by the massive corrosion products would lead to macro-crack generations in the columns, which could serve as extra channels for the water penetration under freeze–thaw condition. Besides, the severe corrosion would also lead to the reduction of reinforcement strength. This then results in a significant decline in bearing capacity of columns. Moreover, due to the higher tensile strength of CFRP strips, the bearing capacities of CFRP strengthened column were obviously higher than those of the GFRP strengthened column.

**Table 2**
Mechanical properties of FRP strip.

| FRP type | Freeze-thaw cycles | $\sigma_t$ (MPa) [COV] | $E_t$ (GPa) [COV] | $\varepsilon_t$ (%) [COV] |
|---|---|---|---|---|
| GFRP | 0 | 1342.62 [0.022] | 99.11 [0.030] | 1.82 [0.040] |
| GFRP | 50 | 1298.41 [0.047] | 101.80 [0.031] | 1.79 [0.040] |
| CFRP | 0 | 3872.20 [0.013] | 245.70 [0.038] | 1.58 [0.023] |
| CFRP | 50 | 3806.50 [0.096] | 245.58 [0.028] | 1.55 [0.013] |

### 3.4. Load-longitudinal strain curve

Two LVDTs were symmetrically fixed on the two sides of columns to measure the longitudinal displacement under eccentric loading. The longitudinal strain, that is, the ratio of longitudinal displacement to the measuring range of LVDTs, was used in this paper. Fig. 7 presents the development trend of longitudinal strain of columns with the load. The load-longitudinal strain curve of CFRP strengthened columns presented similar trend with that of GFRP strengthened columns. While the bearing capacity of columns presents a decreasing trend with the increase of eccentricity, and the load-longitudinal strain curve of columns under eccentric loading were obviously plumper than that of the

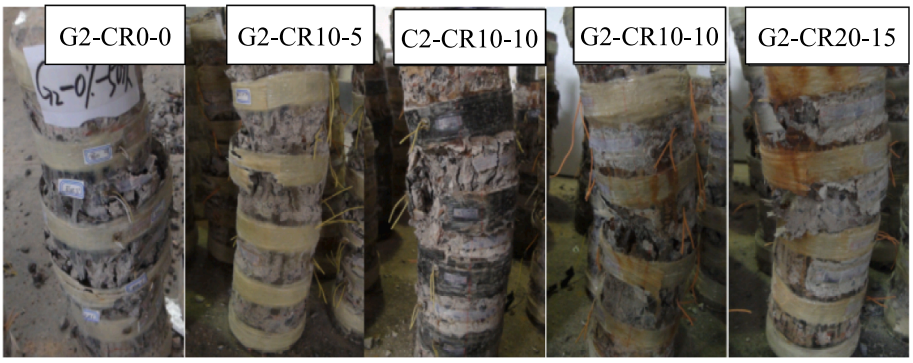


**Fig. 5.** Typical failure mode of columns.

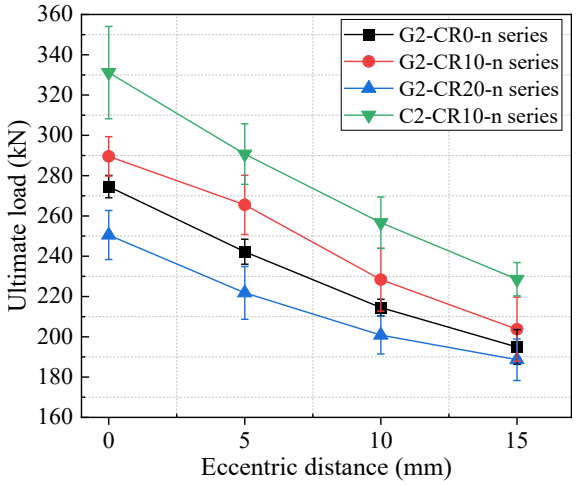


**Fig. 6.** Bearing capacity of FRP strengthened columns.

columns under axial compression loading. For axial compression loaded column, the axial compression load showed a sudden decrease after the ultimate load was reached. While for eccentric loaded columns, the load-longitudinal strain curves had a gradually descending branch after reaching the ultimate load. It should be noted that the longitudinal strain of axial compression loaded columns at ultimate load point was about 0.15 to 0.55 times of that of the eccentric loaded columns. This strain enhancement phenomenon of FRP strengthened circular RC columns was due to the existence of strain gradient under eccentric loading [33–35]. Besides, it was found that the descending stage of load-longitudinal strain curves of GFRP strengthened columns became steeper with increasing reinforcement corrosion degree under the same eccentricity, as shown in Fig. 7(a) to 7(c). This is due to the fact that the tensile capacity and elongation of longitudinal reinforcement is negatively related to the corrosion degree, and pitting corrosion occurs on the surface of reinforcement [21], which results in the decreasing ductility of columns.

## 4. Bearing capacity prediction

Similar to the rectangular RC columns, the failure mode of circular RC columns could also be divided into compressive or tensile failure modes according to the eccentricity. However, the stress of each longitudinal reinforcement that uniformly distributed in the circular column was not equal under the ultimate limit state. The stress state of reinforcement and concrete in the FRP confined circular RC column could be very complex, especially for concrete in the compression zone. The Chinese standard GB 50608 [36] proposed the explicit equations to calculate the sectional capacity of FRP confined circular RC columns. When the longitudinal reinforcements of eccentrically loaded FRP wrapped RC circular columns were uniformly distributed along the column section and the number of longitudinal steel bars were not less than 6, the bearing capacity of columns could be calculated as follows [36]:

$$N \leqslant \psi \alpha_1 f_{rc} A \left(1 - \frac{\sin 2\pi\psi}{2\pi\psi}\right) + (\alpha_c - \alpha_t) f_y A_s \tag{1}$$

$$\alpha_1 = 1.17 - 0.2\frac{f_{rc}}{f_{c0}} \tag{2}$$

where $\psi$ is the ratio of center angle corresponding to the concrete section area in the compression zone to $2\pi$; $f_{rc}$ is the axial compressive strength of FRP wrapped concrete; $f_{c0}$ is the axial compressive strength of unconfined concrete; $A$ is the section area of circular column; $\alpha_c$ is the ratio of section area of longitudinal compression reinforcement to that of all longitudinal reinforcement; $\alpha_t$ is the ratio of section area of longitudinal tensile reinforcement to that of all longitudinal reinforcement; $f_y$ and $A_s$ are the yield strength and section area of longitudinal reinforcement, respectively.

It could be seen from equation (1) that the bearing capacity calculation formula contains two parts: the first part is the bearing capacity of concrete in the compression zone, and the second part is the bearing capacity of longitudinal reinforcement. For concrete in the compression zone, the stress distribution was equivalent to rectangle and $\alpha_1$ in equation (1) is the stress factor. The calculation formula of stress factor adopted by GB 50608 [36] was proposed by Jiang [37], as shown in equation (2). Actually, for circular section columns, both the stress magnitude over the section depth and stress distribution width was variable in the compression zone, and the stress factor was not easy to obtain. The equation (2) was a simplified empirical formula. In addition, for the bearing capacity of longitudinal reinforcement, the equation (1) assumed that the longitudinal reinforcement was yield under the ultimate limit state. However, under small eccentric loading, the whole section of circular column was under compression while part of the longitudinal reinforcement was still in the elastic stage. Therefore, it could be found that the bearing capacity calculation formula proposed by GB 50608 [36] was simplified and part of the stress states of the circular column subjected to eccentric loading was not considered. And the bearing capacity calculation method for circular RC columns subjected to eccentric loading proposed by Chinese standard GB 50010 [38] was similar to that by GB 50608 [36]. Currently, some scholars use the trigonometric integral approach [39] or finite segment element method [40] to calculate the area and location of the centroid of the circular compression block for circular section columns subjected to eccentric loading, and the stress reduction factor of concrete in the compression zone was taken as 0.85 to avoid over estimation of the column strength. These calculation methods were relatively complex and part of the factors was approximate values. In this paper, therefore, to simplify the calculation, the uniformly distributed longitudinal reinforcement was

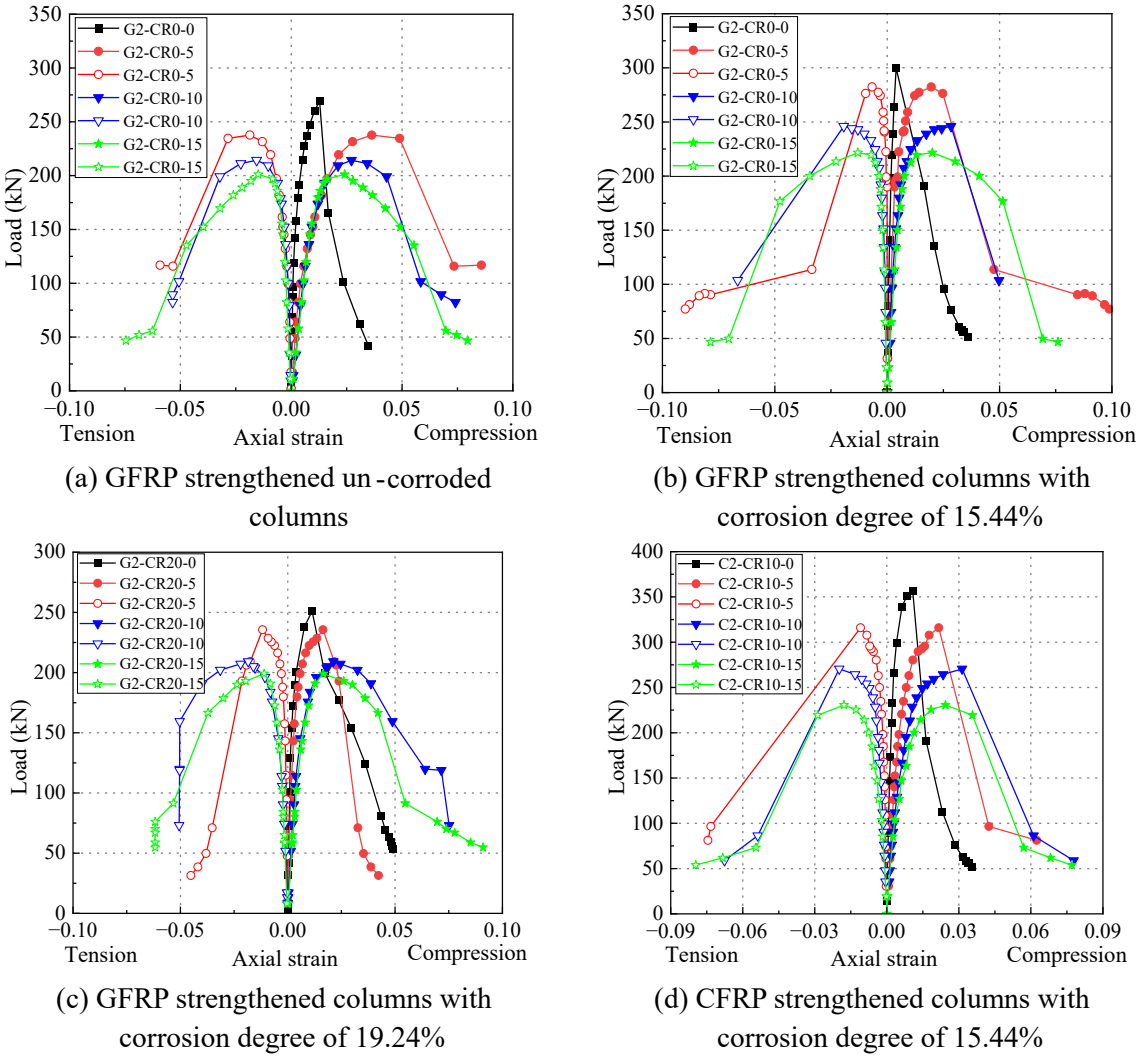


**Fig. 7.** Load-longitudinal strain curve of columns.

assumed to be equivalent to a round steel strip according to the principle of area equality. Similarly, the circular section of column was assumed as rectangular sections (with a height of 86.6 mm and width of 90.7 mm) according to the principle of area and section moment of inertia equality, as shown in Fig. 8. Moreover, based on the stress–strain relationships of FRP partially wrapped concrete and steel bar subjected to combined environmental erosion, the section analysis method was used, and the force state of columns was divided into several cases according to different eccentricities, and a simplified analytical method about the bearing capacity prediction of FRP partially wrapped corrosion damaged columns was proposed.

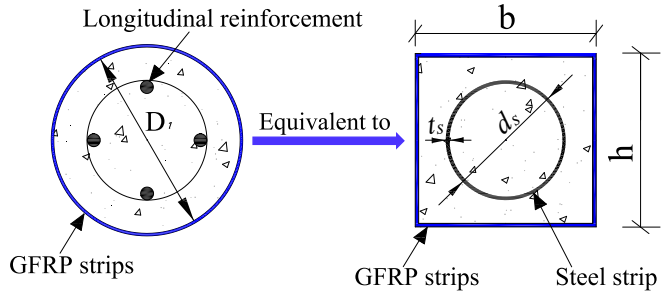


**Fig. 8.** Equivalent conversion of longitudinal reinforcement and circular section.

### 4.1. Stress–strain relationship of FRP partially wrapped concrete under combined environmental erosion

As shown in Fig. 9, the stress–strain model of FRP confined concrete, which was proposed by Lam, was used in this paper [41]. The model expression is given as follows:

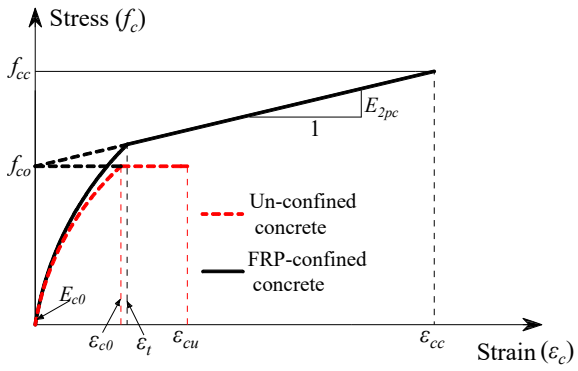


**Fig. 9.** Stress–strain model of FRP confined concrete.

$$f_c = \begin{cases} E_{c0}\varepsilon_c - \dfrac{(E_{c0}-E_{2pc})^2}{4f_{c0}}\varepsilon_c^2 & 0 \leqslant \varepsilon_c < \varepsilon_t \\ f_{c0} + E_{2pc}\varepsilon_c & \varepsilon_t \leqslant \varepsilon_c < \varepsilon_{cc} \end{cases} \tag{3}$$

$$\varepsilon_t = \frac{2f_{co}}{E_{c0}-E_{2pc}} \tag{4}$$

where $E_{c0}$ is the elastic modulus of concrete; $E_{2pc}$ is the slope of ascending straight line; $\varepsilon_{cc}$ is the ultimate compressive strain of FRP confined concrete at the edge of compression zone of column, and expressed as follows [22]:

$$\varepsilon_{cc} = (1.75 + 10 \cdot f_{le}/f_{co}) \cdot \varepsilon_{co} \tag{5}$$

where $f_{le}$ is the lateral restraint stress provided by FRP strips under freeze–thaw erosion environment; $\varepsilon_{c0} = 0.002$ is compressive strain of unconfined concrete [42].

For FRP partially wrapped column, the lateral restraint stress could be calculated as follows [21]:

$$f_{le} = \frac{4k_e \cdot f_{fe} \cdot t_f \cdot b_f}{D \cdot s} \tag{6}$$

where $k_e = 0.586$ is FRP strain efficiency factor [43]; $f_{fe}$ is the tensile strength of FRP strips subjected to freeze–thaw erosion; $t_f$ and $b_f$ are the thickness and width of FRP strip, respectively; $s$ is the spacing between the two FRP strips; $D$ is the diameter of column.

Due to the existence of strain gradient for eccentric loaded column, the restraint effect of FRP will decrease compared to axial compression loaded column. The influence of eccentricity is then taken into consideration for $E_{2pc}$ in the stress–strain model of FRP confined concrete, and the expression is given as follows [22]:

$$E_{2pc} = \frac{f_{cc} - f_{co}}{\varepsilon_{cc}} \cdot \frac{1}{1 + e/h} \tag{7}$$

where $e$ is eccentricity; $h$ is height of equivalent rectangular section; $f_{cc}$ is the axial compressive strength of FRP partially wrapped concrete under erosion environmental. The detailed calculation process of $f_{cc}$ could be found in the published work of authors in Appendix A, and the expression is given as follows:

$$f_{cc} = f_{c0}\left[1 - \left(3.15\omega^2 - 11.73\omega + 13.98\right) \times 10^{-3} \cdot n\right] + \frac{10.6k_e \cdot f_{fe} \cdot t_f \cdot b_f}{D \cdot s} \tag{8}$$

where $\omega$ is the relative ratio of the actual concrete compressive strength to the concrete compressive strength grade of C20, and $\omega = Cm/C20$ ($m \geq 20$); $n$ is the number of freeze–thaw cycles.

### 4.2. Stress–strain relationship of reinforcement under combined environmental erosion

The influence of freeze–thaw erosion on was not obvious for mechanical properties of steel bar reinforced in concrete structures [44]. Therefore, only the influence of chloride erosion on the mechanical properties of steel bar was considered. The ideal elastic–plastic stress–strain relationship of reinforcement was adopted. The expression is as follows:

$$f_s = \begin{cases} E_s\varepsilon_s & 0 \leqslant \varepsilon_s \leqslant \varepsilon_{stc} \\ \sigma_{sc} & \varepsilon_s \leqslant \varepsilon_{sc} \end{cases} \tag{9}$$

where $\varepsilon_{stc} = \sigma_{sc}/E_s$; $E_s$ and $\sigma_{sc}$ are the elastic modulus and yield strength of corroded reinforcement, respectively.

Existing studies [45,46] indicate that the elastic modulus of corroded reinforcement remains unchanged while the yield strength decreases with increasing corrosion degree, and the expression is given as follows:

$$\sigma_{sc} = (1 - \varphi\eta_s) \cdot f_y \tag{10}$$

where $\varphi$ is a constant and taken as 1.1; $\eta_s$ is the corrosion degree; $f_y$ is the yielding strength of un-corroded reinforcement.

### 4.3. Calculation of equivalent rectangular stress of concrete and steel strip

#### 4.3.1. Equivalent rectangular stress of concrete

For FRP confined corroded RC columns under small eccentric loading, the plane section assumption is still applicable [12]. The stress and strain distribution of concrete in equivalent rectangular column section under eccentric loading is presented in Fig. 10. According to the principles of resultant force equality and the action point of resultant force unchanged, the stress distribution of concrete in the compression zone of columns was assumed in rectangular form for calculation convenience.

For a strain state as shown in Fig. 10, the concrete strain at any height of compression zone under ultimate limit state could be calculated as follows:

$$\varepsilon_c = \frac{\varepsilon_{cc}}{x} \cdot y \tag{11}$$

where $x$ is the depth of compression region of concrete; $y$ is the distance from this point to neutral axis.

Substitute equation (11) into equation (3), the following equation could be obtained based on the principle of resultant force equality:

$$\begin{aligned} \alpha f_{c0} \cdot \beta x = D &= \int_0^{\frac{\varepsilon_t}{\varepsilon_{cc}} \cdot x} \left[ E_{c0} \cdot \frac{\varepsilon_{cc}}{x} \cdot y - \frac{(E_{c0}-E_{2pc})^2}{4f_{co}} \left(\frac{\varepsilon_{cc}}{x} \cdot y\right)^2 \right] dy + \int_{\frac{\varepsilon_t}{\varepsilon_{cc}} \cdot x}^{x} \left[ f_{co} \right. \\ &\quad \left. + E_{2pc} \cdot \frac{\varepsilon_{cc}}{x} \cdot y \right] dy \end{aligned} \tag{12}$$

where $\alpha$ and $\beta$ are coefficients of stress and height of rectangular stress block, respectively.

According to equation (12), the following equation could be obtained:

$$\alpha\beta = 1 + \frac{f_{cc} - f_{co}}{2f_{co}(1 + e/h)} - \frac{\varepsilon_t}{3\varepsilon_{cc}} \tag{13}$$

Based on the principle of the action point of resultant force unchanged, the following equation could be obtained:

$$\begin{aligned} x - \frac{\beta x}{2} &= \left\{ \int_0^{\frac{\varepsilon_t}{\varepsilon_{cc}} \cdot x} \left[ E_{c0} \cdot \frac{\varepsilon_{cc}}{x} \cdot y - \frac{(E_{c0}-E_{2pc})^2}{4f_{co}} \left(\frac{\varepsilon_{cc}}{x} \cdot y\right)^2 \right] \cdot y dy + \int_{\frac{\varepsilon_t}{\varepsilon_{cc}} \cdot x}^{x} \left[ f_{co} \right. \right. \\ &\quad \left. \left. + E_{2pc} \cdot \frac{\varepsilon_{cc}}{x} \cdot y \right] \cdot y dy \right\} \Big/ D \end{aligned} \tag{14}$$

By simplifying equation (14), the following equation could be obtained:

$$\alpha\beta \cdot \left(1 - \frac{\beta}{2}\right) = \frac{1}{2} + \frac{f_{cc} - f_{co}}{3f_{co}(1 + e/h)} - \frac{\varepsilon_t^2}{12\varepsilon_{cc}^2} \tag{15}$$

According to equations (13) and (15), the expressions of $\alpha$ and $\beta$ are given as follows:

$$\alpha = \frac{(6 + 3R_\sigma - 2R_\varepsilon)^2}{6(R_\sigma - 2)^2 + 12R_\varepsilon + 12} \tag{16}$$

$$\beta = \frac{(R_\varepsilon - 2)^2 + 2R_\sigma + 2}{6 + 3R_\sigma - 2R_\varepsilon} \tag{17}$$

where $R_\sigma = (f_{cc} - f_{c0})(1 + e/h)/f_{c0}$; $R_\varepsilon = \varepsilon_t/\varepsilon_{cc}$.

Seen from equations (16) and (17), the coefficients $\alpha$ and $\beta$ were related to the mechanical properties of FRP confined concrete and eccentricity. According to the test results, the values of $\alpha$ and $\beta$ of FRP strengthened columns with different eccentricities in this work are presented in Fig. 11, which shows that the FRP type and eccentricity have no significant influences on the value of $\beta$ under the small eccentric loading. Moreover, the value of $\alpha$ of CFRP strengthened columns was

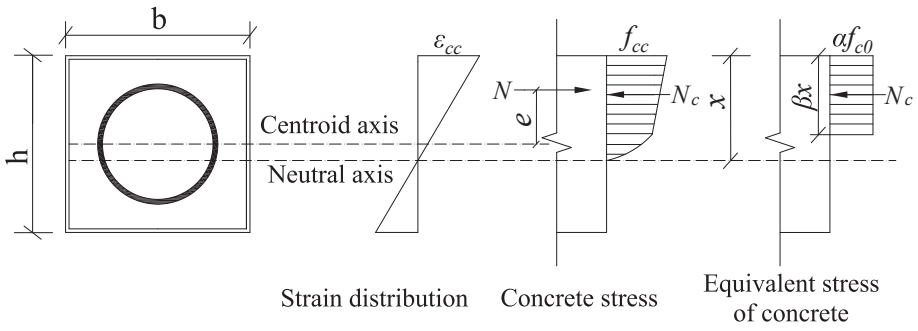


**Fig. 10.** Strain and stress distribution of concrete.

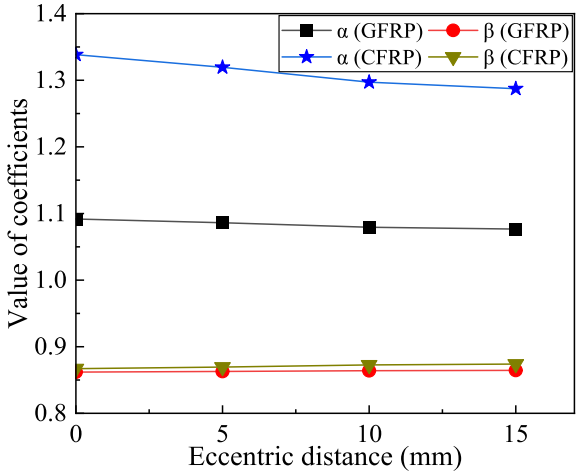


**Fig. 11.** Values of $\alpha$ and $\beta$ of GFRP and CFRP strengthened columns with different eccentricities.

greater than that of the GFRP strengthened columns while both the values of $\alpha$ of GFRP and CFRP strengthened columns slightly decreases with the increase of eccentricity.

#### 4.3.2. Equivalent rectangular stress of steel strip

Fig. 12 presents stress distribution of steel strip in equivalent rectangular column section under eccentric loading. As shown in this figure, the stress of steel strip was distribution in a trapezoidal form in the elastic stage and rectangle form in plastic stage. Referring to the principle of concrete stress equivalence, the stress distribution of steel strip in elastic stage could also be equivalented to a rectangular form. The following equations could then be obtained based on the principles of resultant force equality and the action point of resultant force unchanged:

$$\alpha_s \cdot f_b \cdot \beta_s \cdot x_{sh} = \frac{f_a + f_b}{2} \cdot x_{sh} \tag{18}$$

$$\frac{\beta_s}{2} \cdot x_{sh} = \frac{2f_a + f_b}{3(f_a + f_b)} \cdot x_{sh} \tag{19}$$

where $f_a$, $f_b$, and $x_{sh}$ are the upper bottom, lower bottom, and height of trapezoid distributed stress, respectively; $\alpha_s$ and $\beta_s$ are coefficients of stress and height of equivalent rectangular stress block of steel strip, respectively, and the expressions are given as follows:

$$\alpha_s = \frac{3(f_a + f_b)^2}{4(2f_a + f_b) \cdot f_b} \tag{20}$$

$$\beta_s = \frac{2(2f_a + f_b)}{3(f_a + f_b)} \tag{21}$$

In addition, when the stress distribution of steel strip in elastic stage follows a triangular form, it can be considered as a special case where the upper bottom of the trapezoid is 0. And the values of $\alpha_s$ and $\beta_s$ were taken as 3/4 and 2/3, respectively.

### 4.4. Bearing capacity calculation of column

Since the fiber orientation of FRP strips was the hoop direction of columns in this work, the contribution of FRP confined concrete in tension zone to the bearing capacity of column was not considered. The force state of columns was divided into four cases in accordance with different eccentricities.

#### 4.4.1. Case 1

In case 1, the steel strip is under full section compression. Fig. 13 presents the stress and strain distribution of concrete and steel strip. The depth of compression region is under the state of $(h + d_s)/2 \le x < h$. According to the plane section assumption and adopted geometry, following equations could be obtained:

$$f_a = \left(1 - \frac{h + d_s}{2x}\right) \cdot \varepsilon_{cc} \cdot E_s \tag{22}$$

$$f_b = \sigma_{sc} \tag{23}$$

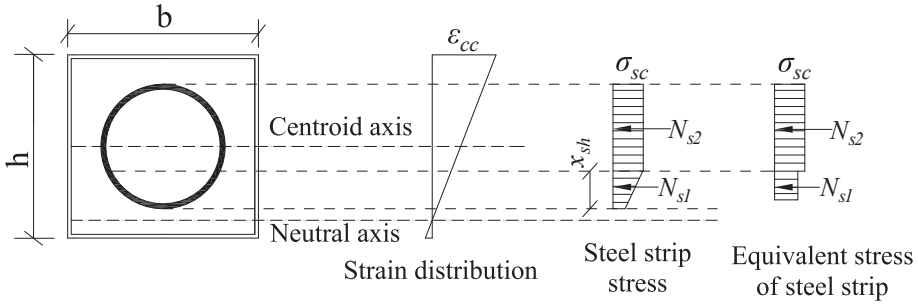


**Fig. 12.** Stress distribution of steel strip.

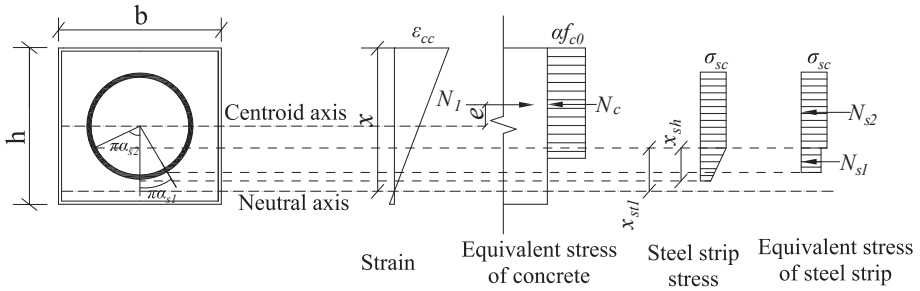


**Fig. 13.** Strain and stress distribution of concrete and steel strip in case 1.

$$x_{sh} = x_{st1} - \left(x - \frac{h + d_s}{2}\right) \tag{24}$$

where $d_s$ is the diameter of round steel strip; $x_{st1}$ is the distance between the position when the steel strip reached yield strength and the neutral axis, as shown in Fig. 13, and calculated as follows:

$$x_{st1} = \frac{\sigma_{sc}}{E_s} \cdot \frac{x}{\varepsilon_{cc}} \tag{25}$$

According to the equilibrium condition of column under ultimate limit state, the force and moment balance equations are given as follows:

$$N_1 = N_c + N_{s1} + N_{s2} \tag{26}$$

$$N_1\left(e + x - \frac{h}{2} - x_{st1} + \frac{\beta_s x_{sh}}{2}\right) = N_c\left(x - \frac{\beta}{2}x - x_{st1} + \frac{\beta_s x_{sh}}{2}\right) + N_{s2}\left(\frac{x}{2} - \frac{x_{st1}}{2} - \frac{h - d_s}{4} + \frac{\beta_s x_{sh}}{2}\right) \tag{27}$$

where $N_1$ is the bearing capacity of column under the state of case 1; $N_c$ is the stress of concrete in compression zone; $N_{s1}$ and $N_{s2}$ are the compressive stresses of steel strip in the elastic and plastic stage, respectively. And the expressions are given as follows:

$$N_c = \alpha f_{c0} \cdot \beta x \cdot b \tag{28}$$

$$N_{s1} = \alpha_s \cdot \sigma_{sc} \cdot A_s(\alpha_{s2} - \alpha_{s1}) \tag{29}$$

$$N_{s2} = \sigma_{sc} \cdot A_s(1 - \alpha_{s2}) \tag{30}$$

where $A_s$ is section area of the steel strip; $2\pi\alpha_{s1}$ is the central angle corresponding to chord length of the intersection between the side length of equivalent rectangular stress of steel strip in elastic stage that close to the neutral axis and steel strip section, and $2\pi\alpha_{s2}$ is the central angle corresponding to chord length of the intersection between the side length of equivalent rectangular stress of steel strip in elastic stage that far from the neutral axis and steel strip section, as shown in Fig. 13.

According to the geometric relationship, the following equations could be obtained:

$$\cos\pi\alpha_{s1} = \frac{d_s/2 - (1 - \beta_s)x_{sh}}{d_s/2} \tag{31}$$

$$\cos\pi\alpha_{s2} = \frac{x - h/2 - x_{st1}}{d_s/2} \tag{32}$$

Here, $\alpha_{s1}$ is taken as 0 when $cos\pi\alpha_{s1} \geq 1$, and taken as 1 when $cos\pi\alpha_{s1} \leq -1$. The value range of other center angles in this paper is the same as $\alpha_{s1}$.

#### 4.4.2. Case 2

In case 2, the steel strip in the compression zone yields while the tension zone is still elastic. Fig. 14 presents the stress and strain distribution of concrete and steel strip. The depth of compression zone could be obtained as:

$$\frac{\varepsilon_{cc} \cdot E_s \cdot (h + d_s)}{2(\sigma_{sc} + \varepsilon_{cc} \cdot E_s)} \leqslant x < \frac{h + d_s}{2} \tag{33}$$

According to Fig. 14, the force and moment balance equations are given as follows:

$$N_2 = N_c + N_{s1} + N_{s2} - N'_{s1} \tag{34}$$

$$N_2(e + x - \frac{h}{2} - \frac{2x_{st1}}{3}) = N_c(x - \frac{\beta x}{2} - \frac{2x_{st1}}{3}) + N_{s2}(\frac{x}{2} - \frac{x_{st1}}{6} - \frac{h - d_s}{4}) + N'_{s1}(\frac{2x_{st1}}{3} + \frac{2x'_{sh}}{3})\ \frac{1}{2} \tag{35}$$

where $N_2$ is the bearing capacity of column under the state of case 2; $N_{s1}'$ is the tensile stress of steel strip in elastic stage.

In this case, the expressions of $N_c$, $N_{s1}$, and $N_{s2}$ were the same as those in case 1. And $N_{s1}'$ should be calculated as follows:

$$N'_{s1} = \alpha_s f'_{sc} A_s \alpha'_{s1} \tag{36}$$

where $f_{sc}'$ is the bottom edge of triangular stress of steel strip in tension zone; $2\pi\alpha_{s1}'$ is the central angle corresponding to chord length of the intersection between the side length of equivalent rectangular stress of steel strip in tension zone that close to the neutral axis and steel strip section, as shown in Fig. 14.

The expression of $f_{sc}'$ is given as follows:

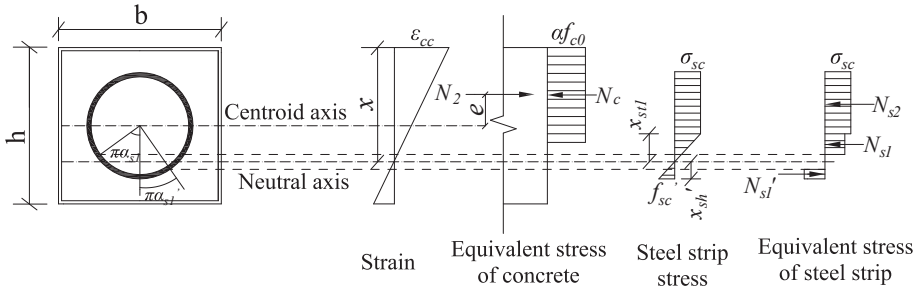


**Fig. 14.** Stress and strain distribution of concrete and steel strip in case 2.

$$f_{sc}^{'} = \frac{x_{sh}^{'}}{x} \bullet \varepsilon_{cc} \bullet E_s \tag{37}$$

where $x_{sh}'$ is the height of triangular stress of steel strip in the tension zone, and $x_{sh}'=h/2 + d_s/2 - x$.

In this case, $2\pi\alpha_{s1}$ and $2\pi\alpha_{s1}'$ satisfied the following geometric relationships:

$$\cos\pi\alpha_{s1} = \frac{x - h/2 - (1-\beta_s)x_{st1}}{d_s/2} \tag{38}$$

$$\cos\pi\alpha_{s1}^{'} = \frac{d_s/2 - \beta_s x_{sh}^{'}}{d_s/2} \tag{39}$$

#### 4.4.3. Case 3

In case 3, both the steel strip in compression and tension zone yield. Fig. 15 presents the stress and strain distribution of concrete and steel strip. The depth of compression zone is under following state:

$$\frac{E_s \cdot \varepsilon_{cc} \cdot (h - d_s)}{2(E_s \cdot \varepsilon_{cc} - \sigma_{sc})} \leqslant x < \frac{E_s \cdot \varepsilon_{cc} \cdot (h + d_s)}{2(\sigma_{sc} + E_s \cdot \varepsilon_{cc})} \tag{40}$$

According to Fig. 15, the force and moment balance equations are given as follows:

$$N_3 = N_c + N_{s1} + N_{s2} - N_{s1}^{'} - N_{s2}^{'} \tag{41}$$

$$N_3(e + x - \frac{h}{2} - \frac{2x_{st1}}{3}) = N_c(x - \frac{\beta x}{2} - \frac{2x_{st1}}{3}) + N_{s2}(\frac{x}{2} - \frac{x_{st1}}{6} - \frac{h - d_s}{4}) + N_{s1}^{'}(\frac{4x_{st1}}{3}) + N_{s2}^{'}(\frac{h + d_s}{4} - \frac{x}{2} + \frac{7x_{st1}}{6}) \tag{42}$$

where $N_3$ is the bearing capacity of column under the state of case 3; $N_{s2}'$ is the tensile stress of steel strip in plastic stage.

In this case, the expressions of $N_c$, $N_{s1}$, and $N_{s2}$ were the same as those in case 2. And $N_{s1}'$ and $N_{s2}'$ should be calculated as follows:

$$N_{s1}^{'} = \alpha_s \sigma_{sc} A_s (\alpha_{s1}^{'} - \alpha_{s2}^{'}) \tag{43}$$

$$N_{s2}^{'} = \sigma_{sc} \bullet A_s \bullet \alpha_{s2}^{'} \tag{44}$$

where $2\pi\alpha_{s2}'$ is the central angle corresponding to chord length of the intersection between the side length of equivalent rectangular stress of steel strip in tension zone that far from the neutral axis and steel strip section, as shown in Fig. 15.

Besides, $2\pi\alpha_{s1}'$ and $2\pi\alpha_{s2}'$ satisfy the following geometric relationships:

$$\cos\pi\alpha_{s1}^{'} = \frac{x - h/2 + (1-\beta_s)x_{st1}}{d_s/2} \tag{45}$$

$$\cos\pi\alpha_{s2}^{'} = \frac{x - h/2 + x_{st1}}{d_s/2} \tag{46}$$

#### 4.4.4. Case 4

In case 4, the steel strip in the compression zone was in elastic stage while the tension zone yields. Fig. 16 presents the stress and strain distribution of concrete and steel strip. The depth of compression zone is under following state:

$$\frac{h}{2} - \frac{d_s}{2} \leqslant x < \frac{E_s \cdot \varepsilon_{cc} \cdot (h - d_s)}{2(E_s \cdot \varepsilon_{cc} - \sigma_{sc})} \tag{47}$$

According to Fig. 16, the force and moment balance equations are given as follows:

$$N_4 = N_c + N_{s1} - N_{s1}^{'} - N_{s2}^{'} \tag{48}$$

$$N_4(e - \frac{h}{2} + x + \frac{2x_{st1}}{3}) = N_c(x - \frac{\beta x}{2} + \frac{2x_{st1}}{3}) + N_{s1}(\frac{2x_{st1}}{3} + \frac{2x_{sh}}{3}) + N_{s2}^{'}(\frac{h + d_s}{4} - \frac{x}{2} - \frac{x_{st1}}{6}) \tag{49}$$

where $N_4$ is the bearing capacity of column under the state of case 4.

In this case, the expressions of $N_c$, $N_{s1}'$, and $N_{s2}'$ are the same as those in case 3. And $N_{s1}$ should be calculated as follows:

$$N_{s1} = \alpha_s \cdot f_{sc} \cdot A_s (1 - \alpha_{s1}) \tag{50}$$

where $f_{sc}$ is the bottom edge of triangular stress of steel strip in the compression zone, and calculated as follows:

$$f_{sc} = \frac{x_{sh}}{x} \cdot \varepsilon_{cc} \cdot E_s \tag{51}$$

Besides, the geometric relationships $2\pi\alpha_{s1}'$ and $2\pi\alpha_{s2}'$ are the same as those in case 3, and $x_{sh}$ should be calculated as follows:

$$x_{sh} = x - \frac{h}{2} + \frac{d_s}{2} \tag{52}$$

### 4.5. Model validation and discussion

For case 1, substitute $x=(h + d_s)/2$ into formulas (26) and (27), the limit of the eccentricity $e_1$ could be calculated. Similarly, substitute $x = \varepsilon_{cc} \bullet E_s \bullet (h + d_s)/2/(\sigma_{sc} + \varepsilon_{cc} \bullet E_s)$, $x = E_s \bullet \varepsilon_{cc} \bullet (h - d_s)/2/(E_s \bullet \varepsilon_{cc} - \sigma_{sc})$, and $x=(h - d_s)/2$ into formulas (34) and (35), formulas (41) and (42), and formulas (48) and (49), respectively. The limit of the eccentricity $e_2$, $e_3$, and $e_4$ for case 2, case 3, and case 4 could be calculated, respectively. Based on the design parameters in this experiment, the limit of the eccentricities of GFRP wrapped column with corrosion degree of 15.44 % were obtained as follows: $e_1 = 12$ mm, $e_2 = 18.7$ mm, $e_3 = 89.7$ mm. And the limit of the eccentricities of CFRP wrapped column with corrosion degree of 15.44 % were obtained as follows: $e_1 = 11.7$ mm, $e_2 = 16$ mm, $e_3 = 96.3$ mm. When the depth of compression zone $x=(h - d_s)/2$, both the GFRP and CFRP wrapped columns were almost in pure bending state and the bearing capacity close to zero. Substitute the eccentricities applied in this experiment into the bearing capacity calculation formulas of corresponding cases, the bearing capacity of columns could then be calculated. Fig. 17 presents the experimental and calculated bearing

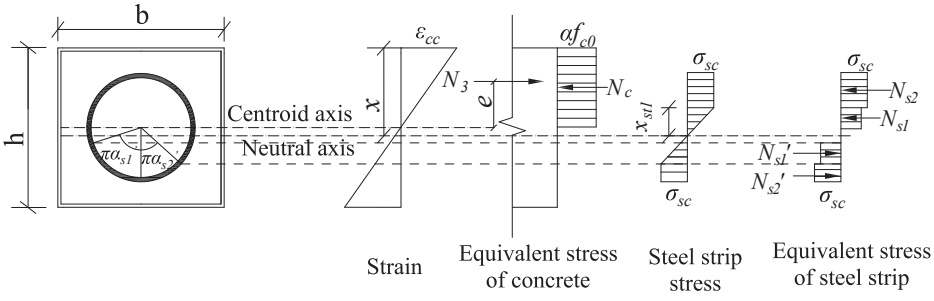


**Fig. 15.** Stress and strain distribution of concrete and steel strip in case 3.

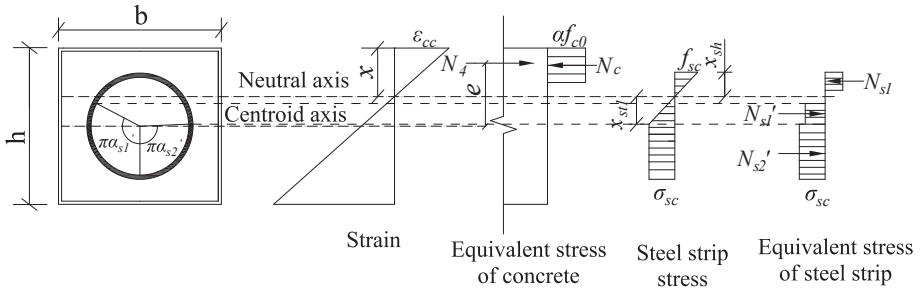


**Fig. 16.** Stress and strain distribution of concrete and steel strip in case 4.

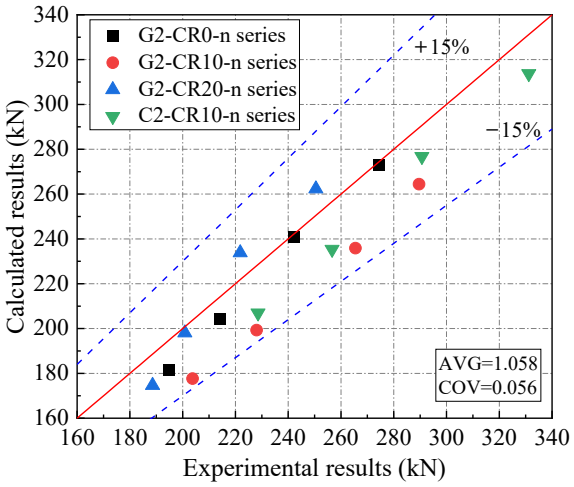


**Fig. 17.** Experimental and calculated results.

capacities of different series columns in this experiment. The average ratio of experimental to calculated results is 1.058 and the COV is 0.056, which confirms the accuracy of the model.

Fig. 18 presents the peak axial force and bending moment (P-M) interaction diagrams of different series columns calculated by the proposed analytical model. For case 1 and case 2, the columns were under compression dominated region, case 3 were transition region, and case 4 were tension dominated region. Fig. 18(a) presents the P-M interaction diagrams of GFRP strengthened column with different corrosion degrees. The size of P-M envelope of GFRP strengthened columns showed a decreasing trend with the increasing corrosion degree, which indicated that the reinforcement corrosion and freeze–thaw erosion plays an significant effect on the capacity of columns regardless of the eccentricity. Under axial compressive loading, the axial force of columns decreased with the increasing corrosion degree. And under pure bending load, the bending moment of columns also showed a decreasing trend with the increasing corrosion degree. Besides, under small eccentric loading, both the axial force and bending moment of columns decreased with the increasing corrosion degree. However, under large eccentric loading, the axial force of columns increased with the increasing corrosion degree under the same bending moment. The main reason was that most of the longitudinal reinforcements were in tension under large eccentric loading, and corrosion would lead to the decreasing tensile stress of reinforcements, thus result in the increasing axial force of columns. The P-M interaction diagrams of GFRP and CFRP strengthened columns with the corrosion degree of 15.44 % are presented in Fig. 18(b). In compression dominated region, the capacity of CFRP strengthened columns was significantly higher than that of GFRP strengthened columns. While under the large eccentric loading, the capacity of CFRP strengthened column gradually reduced to the same level with that of the GFRP strengthened columns with the increase of eccentricity. This was due to the fact that the fiber orientation of FRP strips in this study was along the hoop direction of columns and had no improvement on the tensile properties of concrete under pure bending moment.

## 5. Conclusions

In this work, the mechanical properties of FRP strengthened RC columns under combined environmental erosion were investigated under small eccentric loading conditions. Experimental explorations as well as analytical models were proposed, and the main conclusions are

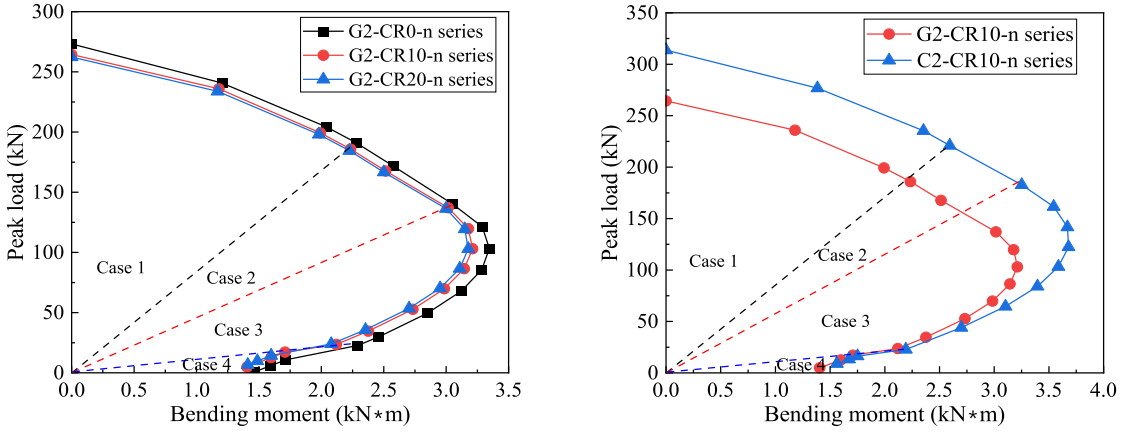


(a) GFRP strengthened columns with different corrosion degrees

(b) GFRP and CFRP strengthened columns with corrosion degree of 15.44%

**Fig. 18.** P-M interaction diagrams of columns.

summarized as follows:

(1) The FRP strengthened corroded RC columns subjected to freeze–thaw cycles exhibits ductile failure regardless of the eccentricity. Tensile failure modes with neat or serrated section dominate for CFRP strips wrapped on the columns, while the GFRP strips adopt the splitting or tearing failure modes.
(2) Both the GFRP and CFRP strengthened columns present a decreasing trend of bearing capacity with the increasing eccentricity, while this effect reduces with the increasing eccentricity. The bearing capacity of GFRP strengthened columns follows a 2-stage behavior, which firstly increases and then decreases, with the increasing corrosion degree. The maximum bearing capacity is reached when the corrosion degree is 15.44 %. The strengthening effect of CFRP is more significant than that of GFRP under small eccentric loading.
(3) The longitudinal strain of axial compression loaded columns at ultimate load point is about 0.15 to 0.55 times of that of the eccentric loaded columns. And the ductility of FRP strengthened corrosion damaged columns decreases with the increasing corrosion degree.
(4) A simplified analytical model about the bearing capacity prediction of FRP partially wrapped damaged RC columns under eccentric loading is proposed. Modeling results agree well with the experimental results.

Due to the limited experimental conditions and time, only the small scale circular columns with diameter of 100 mm were tested in this study. And the concrete strength, number of FRP layers, and freeze–thaw cycles were also unchanged. The future investigations would enrich the relatively limited experimental setups and take into consideration the variations of freeze–thaw cycles, volumetric FRP ratio, concrete compressive strength, and column size to further investigate the applicability of the test results and proposed analytical model in practical scenarios..

## CRediT authorship contribution statement

**Zhiqiang Gu:** Conceptualization, Data curation, Formal analysis, Investigation, Methodology, Writing – original draft, Visualization, Funding acquisition, Project administration. **Congjie Wei:** Conceptualization, Writing – review & editing. **Chenglin Wu:** Supervision, Writing – review & editing. **Danying Gao:** Conceptualization, Funding acquisition, Supervision, Writing – review & editing. **Peibo You:** Investigation, Funding acquisition, Data curation. **Dong Wei:** Investigation, Funding acquisition.

## Declaration of Competing Interest

The authors declare that they have no known competing financial interests or personal relationships that could have appeared to influence the work reported in this paper.

## Data availability

All data related to the present study could be available from the corresponding author upon rational request.

## Acknowledgements

Finical supports provided by National Natural Science Foundation of China (Nos.: 51978629 and 52108207), First Class Project of Yellow River Laboratory (Zhengzhou University) (No. YRL22YL04), Henan Provincial Natural Science Foundation Youth Fund Project (No. 212300410106), and Key Scientific Research Projects of Henan Colleges and Universities (Nos.: 23A570003 and 22A570010) are gratefully acknowledged.

## Appendix A

The explanation about the actual corrosion degree of steel bar in the RC columns and formula derivation of $f_{cc}$ associated with this paper could be found in the published literature of authors, at https://doi.org/10.1016/j.jobe.2022.104883.

## References

[1] Li Q, Dong Z, He Q, Fu C, Jin X. Effects of reinforcement corrosion and sustained load on mechanical behavior of reinforced concrete columns. Materials 2022;15:3590.
[2] Liu Y, Hao H, Hao Y. Blast fragility analysis of RC columns considering chloride-induced corrosion of steel reinforcement. Struct Saf 2022;96.
[3] Rinaldi Z, Di Carlo F, Spagnuolo S, Meda A. Influence of localised corrosion on the cyclic response of reinforced concrete columns. Eng Struct 2022;256.
[4] Belarbi A, Bae S-W. An experimental study on the effect of environmental exposures and corrosion on RC columns with FRP composite jackets. Compos Part B-Eng 2007;38:674–84.
[5] Bae S-W, Belarbi A. Effects of corrosion of steel reinforcement on RC columns wrapped with FRP sheets. J Perform Constr Fac 2009;23(1):20–31.
[6] Suh K, Mullins G, Sen R, Winters D. Effectiveness of fiber-reinforced polymer in reducing corrosion in marine environment. ACI Struct J 2007;104(26):76–83.
[7] Ahmed SK. Strengthening reinforced concrete columns by fiber reinforced polymer (FRP): a general review (Article). J Eng Appl Sci 2018;13(22):9582–96.
[8] Nossoni G, Harichandran RS, Baiyasi MI. Rate of reinforcement corrosion and stress concentration in concrete columns repaired with bonded and unbonded FRP wraps. J Compos Constr 2015;19(5):1–7.
[9] Lee C, Pantazopoulou S, Sheikh S, Thomas MDA, Hearn N, Maalej M, et al. Accelerated corrosion and repair of reinforced concrete columns using carbon fibre reinforced polymer sheets. Can J Civ Eng 2000;27(5):941–8.
[10] Harichandran RS, Baiyasi MI, Nossoni G. Freeze-thaw durability of concrete columns wrapped with FRP and subject to corrosion like expansion. J Mater Civil Eng 2017;29(1):1–7.
[11] Liu X, Li Y. Experimental study of seismic behavior of partially corrosion-damaged reinforced concrete columns strengthened with FRP composites with large deformability. Constr Build Mater 2018;191:1071–81.
[12] Maaddawy TE. Behavior of corrosion-damaged RC columns wrapped with FRP under combined flexural and axial loading. Cement Concrete Comp 2008;30:524–34.
[13] Jayaprakash J, Pournasiri E, De'nan F, Anwar MP. Effect of corrosion-damaged RC circular columns enveloped with hybrid and non-hybrid FRP under eccentric loading. J Compos Mater 2014;49:2265–83.
[14] Tin X, Truc T, Quang t, Thuy T. Effects of steel corrosion to BFRP Strengthened columns under eccentric loading. J Mater Eng Struct 2020;7(4):669–75.
[15] Chotickai P, Tongya P, Jantharaksa S. Performance of corroded rectangular RC columns strengthened with CFRP composite under eccentric loading. Constr Build Mater 2021;268:12134.
[16] Bae S-W, Belarbi A. Effects of various environmental conditions on RC columns wrapped with FRP sheets. J Reinf Plast Comp 2008;29:290–309.
[17] Xf Y, Xia Sh, Lam L, Smith ST. Analysis and behaviour of FRP-confined short concrete columns subjected to eccentric loading. J Zhejiang Univ-SC A 2008;9:38–49.
[18] Wu YF, Jiang C. Effect of load eccentricity on the stress–strain relationship of FRP-confined concrete columns. Compos Struct 2013;98:228–41.
[19] Cao Y, Wu YF, Jiang C. Stress-strain relationship of FRP confined concrete columns under combined axial load and bending moment. Compos Part B-Eng 2018;134:207–17.
[20] Kyaure M, Abed F. Finite element parametric analysis of RC columns strengthened with FRCM. Compos Struct 2021;275.
[21] Gao D, Wei D, Gu Z, Qin D. Compressive behavior of GFRP partially strengthened corroded RC columns subjected to freeze-thaw erosion. J Build Eng 2022;57:104883.
[22] Maaddawy TE. Strengthening of eccentrically loaded reinforced concrete columns with fiber-reinforced polymer wrapping system: experimental investigation and analytical modeling. J Compos Constr 2009;13(1):13–24.
[23] Al-Nimry H, Neqresh M. Confinement effects of unidirectional CFRP sheets on axial and bending capacities of square RC columns. Eng Struct 2019;196.
[24] ACI 440.2R-17. Guide for the design and construction of externally bonded FRP systems for strengthening concrete structures. Farmington Hills, MI, USA: American Concrete Institute (ACI); 2017.
[25] GB/T50082. Test method standard for longterm performance and durability of ordinary concrete:—2009. Beijing: Building Industry Press; 2009.
[26] GB/T50082. Test method for tensile properties of orientation fiber reinforced polymer matrix composite materials:—2009. Beijing: Building Industry Press; 2009.
[27] MOHURD. Standard for test method of mechanical properties on ordinary concrete. Beijing: China Standards Press; 2002.
[28] Cromwell JR, Harries KA, Shahrooz BM. Environmental durability of externally bonded FRP materials intended for repair of concrete structures. Constr Build Mater 2011;25:2528–39.

[29] Apostolopoulos CA, Koulouris KF, Apostolopoulos AC. Correlation of surface cracks of concrete due to corrosion and bond strength (between steel bar and concrete). Adv Civ Eng 2019;2019:1–12.
[30] Chai X, Shang H, Zhang C. Bond behavior between corroded steel bar and concrete under sustained load. Constr Build Mater 2021;310:125122.
[31] Zhou YW, Zheng BW, Zhao DB, Dang LJ, Sui LL, Li DW, et al. Cyclic bond behaviors between corroded steel bar and concrete under the coupling effects of hoop FRP confinement and sustained loading. Compos Struct 2019;224:110991.
[32] Zhang F, Wei F, Wu X, Hu Z, Li X, Gao L. Study on concrete deterioration and chloride ion diffusion mechanism by different aqueous NaCl-MgSO4 concentrations. Buildings 2022;12(1843):1843.
[33] Bisby L, Ranger M. Axial–flexural interaction in circular FRP-confined reinforced concrete columns. Constr Build Mater 2010;24:1672–81.
[34] Lin G, Teng JG. Three-dimensional finite-element analysis of FRP-confined circular concrete columns under eccentric loading. J Compos Constr 2017;21:4017003.
[35] Lin G, Teng JG. Stress-strain model for FRP-confined concrete in eccentrically loaded circular columns. J Compos Constr 2019;23.
[36] GB 50608. Technical standard for fiber reinforced polymer (FRP) in construction: —2020. Beijing: China Planning Press; 2020.
[37] Jiang T. FRP-confined RC columns: analysis, behavior and design. Hong Kong Polytechnic University; 2008.
[38] GB 50010. Code for design of concrete structures:—2010. Beijing: China Architecture & Building Press; 2010.
[39] Abdallah MH, Mohamed HM, Masmoudi R, Moussa A. Analytical modeling of moment-curvature behavior of steel and CFRP RC circular confined columns. Compos Struct 2018;189:473–87.
[40] Al-Nimry HS, Al-Rabadi RA. Axial-flexural interaction in FRP-wrapped RC columns. Int J Concr Struct M 2019;13(1):1–19.
[41] Zeng JJ, Lin G, Teng JG, Li LJ. Behavior of large-scale FRP-confined rectangular RC columns under axial compression. Eng Struct 2018;174:629–45.
[42] GB50010-2015. Code for design of concrete structures. Beijing: China Architecture & Building Press; 2015.
[43] Lam L, Teng JG. Design-oriented stress–strain model for FRP-confined concrete. Constr Build Mater 2003;17:471–89.
[44] Xu S, Li A, Ji Z, Wang Y. Seismic performance of reinforced concrete columns after freeze–thaw cycles. Constr Build Mater 2016;102:861–71.
[45] Song L, Yu Z. Fatigue performance of corroded reinforced concrete beams strengthened with CFRP sheets. Constr Build Mater 2015;90:99–109.
[46] Zhang W, Song X, Gu X, Li S. Tensile and fatigue behavior of corroded rebars. Constr Build Mater 2012;34:409–17.